Decoupling of rates of protein synthesis from cell expansion leads to supergrowth

Benjamin D. Knapp[1,2], Pascal Odermatt[1,3], Enrique R. Rojas[3,4], Wenpeng Cheng[5], Xiangwei He[5], Kerwyn Casey Huang[2,3,4,6,7,*], and Fred Chang[1,*]

[1]Department of Cell and Tissue Biology, University of California, San Francisco, San Francisco, CA 94143

[2]Biophysics Program, Stanford University, Stanford, CA 94305, USA

[3]Department of Bioengineering, Stanford University, Stanford, CA 94305, USA

[4]Department of Biochemistry, Stanford University School of Medicine, Stanford, CA 94305, USA

[5]Life Sciences Institute, Zhejiang University, Hangzhou, Zhejiang, China, 310027

[6]Department of Microbiology and Immunology, Stanford University School of Medicine, Stanford, CA 94305, USA

[7]Chan Zuckerberg Biohub, San Francisco, CA 941586

[*]To whom correspondence should be addressed:

Fred Chang

513 Parnassus Avenue, HSW616

San Francisco, CA 94143 USA

Phone: +1 (415) 476-8922

E-mail: fred.chang@ucsf.edu

Kerwyn Casey Huang

Shriram Center, Room 007 MC: 4245

443 Via Ortega

Stanford, CA 94305-4125 USA

Phone: +1 (650) 721-2483

E-mail: kchuang@stanford.edu

ABSTRACT

Cell growth is a complex process in which the biosynthesis of cellular components must be coordinated with increases in cell size in order to maintain their concentrations. In many cell types, the steady-state growth rate is proportional to cell size such that larger cells grow proportionally faster than smaller cells. Little is known about the mechanisms coordinating biosynthesis, cell volume, and cytoplasmic density. Here, we reveal a global mechanism for proteome homeostasis by transiently decoupling protein synthesis from volume growth rate in the fission yeast *Schizosaccharomyces pombe*. Rapid osmotic oscillations strongly inhibited growth, but when oscillations were terminated cells subsequently underwent a period of "supergrowth" in which growth was significantly faster than steady-state growth for multiple generations. Protein concentrations and cytoplasmic density increased steadily during oscillations, and gradually decreased to steady-state values during supergrowth. Transient growth inhibition by disabling the secretory pathway produced similar behaviors to osmotic oscillations. The accumulation of biomass was responsible for driving subsequent rapid growth, yielding a homeostatic mechanism for maintaining global protein concentration.

INTRODUCTION

Proliferating cells generally increase their biomass and volume during the cell cycle before dividing. Although much is understood about how duplication of certain cellular components such as the chromosomes is accomplished, much less is known about how the proteome itself is duplicated. The concentrations of many proteins are thought to be maintained during cell growth [1-3]. While global mechanisms of proteome homeostasis have been identified [4], it is unknown the extent to which the concentrations of individual proteins are coordinated with cell volume [5], whether this coordination can be altered, and the effects of such a perturbation.

The rate of cellular growth, which we define here as the increase of cellular volume, is determined by numerous factors. The biosynthesis of cellular components has been speculated to set growth rate, as decreasing protein translation, for instance, can slow or halt growth. The rate of cellular growth is also affected by cell size; many organisms, including bacteria, fungi, and mammalian cells, exhibit exponential growth [6,7] in which the absolute growth rate at steady-state is proportional to cell size. Although the mechanism(s) for achieving exponential growth remains to be determined, it may arise from the scaling of the biosynthetic machinery with cell size: if protein synthesis is coupled to cell size, and cell size is dictated by protein concentration, then exponential growth will result.

The fission yeast *Schizosaccharomyces pombe* is an established model for cell-cycle regulation and growth. The simple, rod-shaped morphology and regular growth and division patterns of these cells make them highly amenable to quantitative studies. During their cell cycle, *S. pombe* cells exhibit polarized tip growth at one or both cell tips during interphase [8,9], and growth halts during mitosis and cytokinesis [10,11]. Like other tip-growing cells, the growth of the cell surface is directed by polarity machinery that ultimately mediates remodeling and insertion of new cell wall at the cell tips. Growth of the surface is further impacted by mechanical factors, such as the turgor pressure due to osmolyte concentration imbalances across the membrane that expands the elastic cell wall [8,10]. While exponential volume growth at the single-cell level has been observed in many cell types, whether individual fission yeast cells exhibit such behavior has been a source of controversy for decades; the current consensus is a bilinear growth behavior with an increased slope later in the cell cycle [11-16].

Biomass synthesis (largely driven by protein synthesis) and volume increase (driven by membrane and cell-wall synthesis) must be coordinated during growth, but it is unknown how this fundamental coupling is achieved. Here, we present multiple ways of uncoupling the coordination between biomass and volume in *S. pombe* cells, and thus provide new insights into the role of proteome homeostasis in cell growth. We first establish that fission yeast cells exhibit cell size-dependent, exponential growth for a large fraction of the cell cycle. Through manipulation of turgor pressure or secretion, we decouple the rate of global protein synthesis from growth rate. These conditions produce a global excess of proteins within the cytoplasm, which in turn results in an extended period of extremely rapid growth. These findings thus provide new insights into the role of cytoplasmic density in cell growth and proteome homeostasis, whereby the rapid expansion of dense cells accelerates the re-equilibration of protein concentrations.

RESULTS

Fission yeast cells grow exponentially during a large fraction of the cell cycle

To determine the growth behavior of individual *S. pombe* cells, we imaged cells in time lapse in microfluidic chambers and implemented automated image analysis methods to quantify cellular dimensions at subpixel resolution (Figure 1A, S1A; Methods). In agreement with previous studies, these rod-shaped cells elongated from ~8 μm to 14 μm before entering mitosis (Figure 1B, S1B), and maintained a constant width of ~4 μm (Figure 1B, S1C). Instantaneous growth rates (defined as dL/dt, where L is cell length) of wild-type cells ranged from 2-5 μm/h at 30 °C (Figure 1C), with cell length highly correlated with elongation rate, indicating that growth rate accelerates during the cell cycle. In purely exponential growth, absolute growth rate scales linearly with cell size, hence $\dot{e} = \frac{1}{L}\frac{dL}{dt}$ (size-normalized growth rate) is a constant. Quantification of $\dot{e}$ revealed that fission yeast growth during the cell cycle is organized into at least three phases (Figure 1D): (I) growth acceleration for the first ~10-20% of the cell cycle (immediately after cell separation), (II) exponential growth for the majority of interphase, in which $\dot{e} = 0.35 \pm 0.06$ h^{-1} (corresponding to doubling biomass during interphase in 2.0±0.3 h), and (III) deceleration to zero growth in mitosis and cytokinesis. These data are inconsistent with simple linear or bilinear growth models (Figure S2). We further tested the effect of cell size on growth rate by analyzing abnormally large cells (*cdc25-22* cells at the semi-permissive temperature 30 °C, which divide at 30±4 μm in length). These large cells grew much faster than wild-type cells and followed a similar scaling of single-cell elongation rate with size, with a size-normalized growth rate $\dot{e}$ of 0.30 ± 0.05 h^{-1} (Figure 1C, S1D,E). These findings establish exponential growth behavior in fission yeast, with absolute growth rates that scale with cell size over a wide range of volumes.

Cells grow slowly during oscillatory osmotic shocks, and exhibit super-fast growth upon exit from oscillations

In terms of the mechanics of cell growth, internal turgor pressure provides physical force for expansion of the cell wall to increase cellular volume. Fission yeast cells have a thick (~200 nm), elastic cell wall inflated by high turgor pressures of ~1.5 MPa (15 atm) [10,17]. Examining the effects of adding the osmotic agent D-sorbitol (hereafter sorbitol) to the media has proven useful

for probing the mechanical effects of reducing turgor pressure [10,18-20]. We investigated the effect of mechanical perturbations on cell growth using osmotic oscillations in repeated cycles of hyper- and hypoosmotic shocks (Methods) [21]. We exposed *S. pombe* cells in a microfluidic device to repeated switches between rich medium (YE5S) and YE5S+0.5 M D-sorbitol (Figure 2A, S3A). In these initial experiments, we applied 24 oscillatory cycles of 0.5 M sorbitol shocks with a 10-min period for 4 hours, then subsequently followed cells in YE5S media without sorbitol. Each acute addition of 0.5 M sorbitol caused rapid water efflux, loss of turgor pressure, and shrinkage in volume by ~20%, with mean longitudinal and radial contractions in cell size of 3.5% and 7%, respectively (Figure 2B) [10]. During each 5-min hyperosmotic period, cells partially re-inflated, dependent on osmotic adaption mechanisms (Figure 2B, S3B). Upon hypoosmotic shifts back to YE5S medium without sorbitol, cells rapidly returned to their normal width in the absence of shocks (Figure 2B, S3B), suggesting that *S. pombe* cells can rapidly downregulate turgor pressure to a preferred value when envelope stresses increase above a certain point.

Over the course of 4 hours of these osmotic cycles, cells remained viable and continued to grow and divide (Movie S1, Figure S3C). However, the mean growth rate was lower than that of control cells: growth initially slowed (Figure 2C) for the first ~2 h (to <0.06 h^{-1}, Figure 2D), followed by adaptation to the oscillations after ~3 h that resulted in a size-normalized growth rate increase to ~0.2 h^{-1} (Figure 2D). When cells were returned after the cycles of osmotic oscillations to YE5S without any sorbitol, they grew unusually fast, with tip growth rates >8 μm/h (population mean 6.5±0.9 μm/h), almost two-fold higher than mean control tip growth rates (3.8 μm/hr, Figure 2C); we refer to this period of unprecedented rapid growth as "supergrowth." Size-normalized growth rates indicated that cells were growing abnormally rapidly for their size ($\dot{e} = 0.6$ h^{-1} vs. 0.35 h^{-1} for control cells, Figure 2D). These growth behaviors were highly stereotypical throughout the population (>96% cells, 49/51), and were substantially faster than any previously reported growth rates for fission yeast. Acceleration began by 15 minutes after exit from oscillations (Figure 2C), and growth rate reached a peak just before cells entered mitosis (Figure 2C, S4A). Elevated growth rates persisted for 2-3 generations (~4 hours, Figure 2C,D, S4B), but in each cell cycle, the rate decreased in a step-wise manner from the previous generation even though cells still exhibited exponential growth (Figure S4B,C). Growth still decelerated normally during mitosis and cytokinesis. Interestingly, the initial acceleration

151 phase of the cell cycle (Figure 1D) was largely absent during supergrowth (Figure S4B),
152 suggesting that cells were primed for exponential growth immediately after division.
153
154 Despite the large changes in growth rate during and after the oscillations, cell morphology and
155 size were remarkably normal. Cells exhibited tip growth during interphase without large
156 changes in cell width or tip shape (Figure S5). Importantly, cells entered mitosis at the normal
157 cell length of 14 μm during oscillations and during supergrowth despite a >10-fold range in
158 growth rates, indicating that changes in growth rate did not affect cell-size control (Figure 2E).
159 During supergrowth, cell-cycle periods were shorter because due to a decrease in the duration of
160 interphase, but the durations of mitosis and cytokinesis were normal, indicating that not all
161 cellular processes were sped up (Figure S4C,D). These data suggest that cell size and the periods
162 of cell division are controlled independently of growth rate.
163
164 To determine the requirements for supergrowth, we examined its dependence on oscillation
165 parameters (amplitude, period, number of periods). We systematically varied each parameter
166 around our baseline values (0.5 M, 10-min period, 24 periods), keeping the other two
167 parameters fixed. In general, the maximal supergrowth rate increased gradually with increasing
168 amplitude, period, or number of periods (Figure 2F). Single shocks were generally not sufficient
169 (Figure 2Fii). Oscillations with 1 M sorbitol, which caused ~50% volume loss, resulted in a near-
170 cessation of growth during oscillations, but then subsequently led to rapid supergrowth (Figure
171 2Fiii). These data suggest that growth and cell-cycle progression during oscillations are not
172 required for supergrowth. The graded effects suggest that the rapid growth state is not regulated
173 by an all-or-nothing switch, but rather accumulates over time during the osmotic shifts.
174
175 ***Supergrowth is independent of established osmotic stress and growth pathways***
176 To probe the mechanism underlying supergrowth, we considered two non-exclusive models. The
177 first model involves the osmotic stress-response pathway, which could signal to growth
178 pathways to regulate growth rate. The second model is based on material storage, in which
179 components important for growth accumulate during periods of slow volume expansion because

180 biosynthesis does not slow commensurately with growth rate. The excess of these materials
181 upon exit from oscillations could then drive the subsequent supergrowth.
182
183 As an initial test of the signaling model, we assayed various mutants for their ability to undergo
184 supergrowth. We assessed strains lacking Sty1 and Pmk1 (MAP kinases at the hub of the
185 pathways that response to osmotic, cell-wall, and other environmental stresses) [22,23]; Gpd1,
186 which regulates glycerol synthesis during turgor adaptation to osmotic stresses [19,22]; and Cch1, a
187 calcium channel involved in response to cell-wall stresses [24]. We also queried regulators in the
188 TOR pathway, a central regulator of growth: Ssp2 (an AMPK-like protein kinase that regulates
189 TORC1 activity) [25,26] and Gad8 (an AGC protein kinase effector of TORC2) [27]. All these mutants
190 exhibited supergrowth responses similar to that of wildtype after oscillatory osmotic shock
191 (Figure S6). Ribosomal mutants with slower basal growth rates showed a proportional
192 supergrowth response (Figure S6). Thus, these signaling pathways regulating cellular responses
193 to stress, turgor, and growth are not required for supergrowth.
194
195 ***The proteome globally increases in concentration during osmotic oscillations***
196 The material storage model predicts that components important for growth rise in concentration
197 during oscillations. As an initial test, we monitored a fluorescent protein marker, E2-mCrimson
198 expressed from the *ACT1* (actin gene) promoter. E2-mCrimson is stable and folds relatively
199 rapidly [28]. Under normal growth, mCrimson intensity remained approximately constant
200 throughout the cell cycle (Figure S7A), indicating that this marker is produced at a rate
201 proportional to volume growth rate (Figure S7B), the expected behavior for many native
202 proteins. In contrast, during osmotic oscillations, mCrimson fluorescence concentration
203 increased, rising linearly to ~50% above normal levels after 4 h of 10-min, 500-mM oscillations
204 (Figure 3A-C). When cells entered supergrowth, mCrimson intensity progressively decreased
205 back to wild-type levels over 2-3 generations (Figure 3A-C), similar to the time scale for
206 restoration of normal growth rates.
207
208 To investigate why mCrimson accumulates during osmotic oscillations, we computed the rates of
209 mCrimson production and compared to growth rate. During oscillations, the rate of mCrimson
210 production remained close to normal levels even though cells grew in volume at a much slower

211 rate than normal (Figure S7D). Thus, mCrimson increased in concentration not because of a large
212 increase in protein production, but because of a failure to decrease protein production as much
213 the reduction in volume growth rate.
214
215 We also examined how mCrimson concentration relaxed to equilibrium levels during
216 supergrowth. In this phase, the cells grew in volume much faster than mCrimson production
217 (Figure S7D). Much of this decrease in concentration can thus be explained by a dilution
218 mechanism, which is enhanced by the rapid growth. The rate of "production" was also even
219 lower than normal levels (Figure S7D), which may reflect decreased protein synthesis or
220 increased degradation rates. Calculations using our growth-rate measurements to predict the
221 decay constant of mCrimson fluorescence, assuming steady-state production after oscillations,
222 indicated that at least 75% of the fall in mCrimson levels relative to controls can be explained by
223 dilution during growth. These findings highlight dilution by rapid growth as a mechanism
224 contributing to protein homeostasis.
225
226 Next, we determined whether native cellular proteins also increase in concentration during
227 oscillations. We imaged fluorescently tagged proteins representing a variety of cellular
228 processes, such as metabolism, chromosomal organization, cell-size control, and cell growth
229 (Figure 3D, Table S1). These proteins all maintained a constant concentration during normal
230 growth. Much like E2-mCrimson, the concentrations of many of these cellular proteins increased
231 during 4 hours of 10-min, 0.5 M osmotic oscillations, and then returned gradually to normal
232 during supergrowth (Figure 3D). No aggregates of these tagged proteins were observed. Similar
233 changes in intensities were observed for fusions to various fluorescent proteins (Figure 3D),
234 suggesting that the behavior was not an artifact of any particular fluorescent protein. Among the
235 different protein fusions, there was a large range of behavioral variation, with different rates of
236 increase and decrease during oscillations and supergrowth. Impressively, some proteins
237 accumulated by ~100% during oscillations. In contrast, a subset of proteins displayed modest or
238 no increases in concentration during oscillations. For example, the concentration of histone H2A
239 was relatively steady throughout the experiment (Figure 3D), perhaps reflecting the fact that the
240 amount of DNA is not increasing abnormally in these cells. The cell-size sensor Cdr2 also
241 increased only modestly during oscillations (Figure 3D), consistent with the maintenance of size

242 control. Ribosomal proteins also showed only modest increases (Figure 3E; see section below).
243 These findings suggest that osmotic oscillations caused large changes in the concentrations of a
244 significant subset of cellular proteins.
245
246 We next employed two complementary methods to measure the global state of cellular
247 components. Staining of individual cells for total protein with fluorescein isothiocyanate (FITC)
248 showed a similar rise and fall, with a mean 20% increase during 2 hours of osmotic oscillations
249 (Figure 3F), while DNA concentration remained constant (Figure S8). Quantitative-phase
250 imaging (Methods) showed that intracellular density, as measured from the diffractive index of
251 the cell, also exhibited a ~10% and 20% increase during 0.5-M and 1-M oscillations, respectively
252 (Figure 3G). Both measurements were in approximate agreement with the average increases in
253 protein concentrations (Figure 3D). Thus, osmotic oscillations clearly produce global changes in
254 protein concentration and cytoplasmic density.
255
256 Other oscillation regimes induced even larger increases in protein concentration. For instance,
257 over the course of 48 oscillation cycles with 1 M sorbitol, cells halted growth and accumulated
258 150% higher mCrimson concentrations (Figure S9). These additional oscillatory cycles of 1M
259 sorbitol displayed no sign of saturation in linear concentration accumulation (Figure S9B),
260 suggesting that even higher increases are likely possible.
261
262 We sought to determine if a simple model of growth kinetics could quantitatively predict such a
263 linear increase during growth inhibition. Experimental measurements have shown that
264 translational efficiency $\mu = \lambda_1 \frac{1}{V}\frac{dV}{dt} + \lambda_o$ contains a growth-dependent and growth-independent
265 component λ_0 [29], which leads to a prediction of steady-state growth rate that is within 30% of
266 experimental measurements (see Supplementary Information for more details). In our
267 experiments with 1-M oscillatory shocks, growth halts completely and ribosome concentration is
268 constant. In this scenario, our model predicts that the baseline translational efficiency λ_0 [29]
269 results in accumulation of biomass M at a constant rate $dM/dt = \lambda_0 R$, where R is the ribosome
270 abundance. Hence, M is predicted to increase linearly during osmotic shock oscillations, at a
271 reduced rate relative to unperturbed growth that yields a ~12% increase over 4 hours, similar to

our experimental measurements (Figure 3G). Taken together, our experimental measurements and theoretical model indicate that oscillations and supergrowth represent periods of decoupling of protein production and cell expansion, and lead to profound accumulation of intracellular proteins.

Increased protein concentrations drive supergrowth

Next, we asked whether the increased concentration of proteins is responsible for supergrowth. First, further analysis of our extensive exploration of oscillation parameters revealed that the maximal supergrowth rate was highly correlated with the observed increase in mCrimson concentration during oscillations (Figure 4A, $r = 0.85$). Second, we tested whether the increase of protein concentration is necessary for supergrowth. To globally inhibit protein synthesis, we treated cells with 100 μg/mL cycloheximide [30] during oscillations, and then washed out the inhibitor upon exit from oscillations. These cycloheximide-treated cells recovered to near-normal growth rates but never achieved supergrowth (Figure 4B). Thus, efficient protein translation during oscillations is required for supergrowth.

Finally, we tested whether the accumulation of growth materials during oscillations is sufficient to drive growth in the absence of new protein synthesis. For control cells that were not exposed to oscillatory shocks, cycloheximide treatment caused a rapid cessation in cell growth. In contrast, cells that had been exposed to oscillations still grew substantially, at ~3-fold faster growth rates than control cells for 2 h (Figure 4C,D). Cells after oscillations also reestablished steady-state growth rates upon removal of cycloheximide more quickly (Figure 4C). Collectively, these results support the storage model in which cells with accumulated components are able to undergo some growth even in the absence of new protein synthesis.

Effect of ribosomal concentration, cell wall synthases, and turgor pressure on supergrowth

To probe whether the up-regulation of particular cellular processes drives supergrowth, we assessed three candidates involved in growth regulation: ribosomes, the cell-wall biosynthetic machinery, and turgor pressure. We monitored ribosomal protein abundances in single cells using ribosomal protein-GFP fusions expressed from their endogenous promoters (Methods) and

302 found that their steady-state concentrations were relatively constant (Figure 3E). The
303 concentrations of these ribosomal proteins increased only modestly during oscillations (from 0-
304 20%) (Figure 3E) and then quickly reverted to baseline levels during supergrowth. Some
305 ribosomal proteins displayed nearly constant concentration throughout the experiment (Figure
306 3E, S10), indicating that their production rates decreased and increased concurrently with the
307 growth rate. Thus, rapid supergrowth is not caused by a large increase in ribosome
308 concentration.
309
310 As cell-wall assembly likely limits the rate of cell expansion, a candidate factor for controlling
311 cell-wall growth is the major cell-wall glucan synthase Bgs4. Bgs4 is a trans-membrane protein
312 that localizes to growing cell tips during interphase and to the developing septum during
313 cytokinesis [31]. During the oscillations, as cells grew slowly (Figure S11A), Bgs4 puncta were
314 delocalized across the cell membrane (Figure S11B), consistent with the general depolarization
315 of actin and Cdc42 seen in the osmotic-shock response [31-33]. Bgs4 intensities at cell tips
316 decreased by 50%, although total Bgs4 concentration gradually increased (by ~50%) during this
317 period (Figure 3D). Upon exit from oscillations, Bgs4 rapidly repolarized to the cell tip, and tip
318 intensities rose to more than 50% more than in control cells within 30-45 min (Figure S11B).
319 The amount of Bgs4 at the cell tips strongly correlated with the growth rate in these experiments
320 (r = 0.95) (Figure S11C). It is likely that such increases in the levels of Bgs4 and additional
321 polarity factors contributing to cell wall growth collectively contribute to rapid growth. These
322 results reveal mechanistic insight into why cell growth slows down during osmotic shock
323 oscillations and how polarized growth is rapidly established after oscillations.
324
325 Another potential contributor to supergrowth could be an increase in turgor pressure that may
326 arise from increased cytoplasmic density. We examined turgor pressure by measuring cell
327 width, as changes in turgor pressure are expected to lead to concurrent reversible swelling in
328 cell width independent of tip elongation. Although cell widths increased slightly during osmotic
329 oscillations, they did not decrease during supergrowth as cytoplasmic density decreases (Figure
330 S5A, S12). These data indicate that the small width increases during oscillations are not
331 reversible and thus may arise from delocalized cell wall synthesis (Figure S11B,C) [32], rather than

332 from increases in turgor pressure. In sum, turgor pressure is unlikely to increase substantially
333 during supergrowth, and is not the driver of the increase in growth rate during supergrowth.
334
335 ***Transient inhibition of protein secretion also drives subsequent supergrowth***
336 Our model predicted that other perturbations that transiently inhibit cell volume growth would
337 also lead to proteome accumulation and subsequent supergrowth. One way of stopping growth
338 and increasing buoyant density is through inhibition of secretion, as shown initially in budding
339 yeast [34]. To halt secretion, we treated mCrimson-expressing cells for 4 hours with 100 μg/mL
340 brefeldin A (BFA), which inhibits protein transport from the endoplasmic reticulum to the Golgi
341 apparatus [35,36]. Cells exhibited a rapid decrease in growth rate to essentially zero throughout
342 BFA treatment, during which time mCrimson concentration increased approximately linearly
343 (Figure 4E). Many cells eventually died, but the 45% of cells that survived the treatment
344 exhibited supergrowth upon BFA wash out (Figure 4E) with growth-rate trajectories similar to
345 those observed after 0.5 M sorbitol oscillatory osmotic shocks (Figure 2D). Thus, rather than just
346 a response to osmotic stress, supergrowth and proteome accumulation can be produced by other
347 treatments that limit volume expansion without proportional inhibition of protein synthesis.

DISCUSSION

Here, our interrogation of the growth response of *S. pombe* cells to osmotic perturbations has revealed unexpected insights into the relationships between cell size, growth, and biosynthesis. In investigating the basis for supergrowth, we find that these unprecedented rapid growth rates arise from a decoupling of biosynthesis and volume expansion. During the osmotic oscillations, volume expansion is impaired far more than biosynthesis, which leads to global accumulation of cellular components inside the cell. Release from these conditions then results in abnormally rapid growth that drives an accelerated return to normal proteome concentrations relative to dilution. Our results thus support a model in which rapid growth is driven by the accumulation of cellular materials. This effect of material storage on growth rate may be connected with the mechanisms underlying the near-universal scaling of growth rate with cell size (exponential growth) observed under steady-state environmental conditions across the kingdoms of life. In the simplest interpretation, cells in supergrowth grow rapidly because they have the internal resources of a larger cell. Whether the cellular materials that promote growth are some subset of the cytoplasmic constituents, or the entire collection, remains to be seen. Our data suggests that growth rate is set by a combination of cellular processes, including the biosynthetic machinery, metabolism, and cell-wall assembly, rather than by a single component such as ribosomes.

This work reveals that relatively simple manipulations can decouple cell growth and protein synthesis, yielding mechanistic insights into how these fundamental processes are normally coordinated. As concentrations of many proteins do not vary greatly during steady-state growth, it has been speculated that extensive feedback mechanisms exist for protein homeostasis; for instance, increased concentration of a certain protein may inhibit its own translation or transcription through a signaling pathway that senses its concentration, leading to a decrease back to normal levels; such a protein-specific mechanism has been suggested for tubulin homeostasis for instance [37]. In this scenario, we speculate that osmotic oscillations lead to breakdown of the putative feedback mechanisms, possibly because of the rapid changes in cell size and concentrations. However, our findings also raise a second, simpler possibility in which signaling feedback mechanisms may not exist for many proteins [38-40]. We speculate that volume expansion itself could act as a homeostatic mechanism, wherein biomass increases largely independent of volume and small variations in cytoplasmic protein concentrations are brought

back into balance by a correction in short-term volume growth rate. Abnormal increases in protein concentrations would drive faster growth than synthesis, which would decrease their concentration in part through dilution, similar to what we observe during supergrowth. A decrease in protein concentration would lead to slowed growth, allowing protein concentration to build back up. Our experiments were able to reveal such a mechanism for the coordination of growth and volume, because they allowed us to uncouple this coordination and examine the recovery process.

Such a mechanism however may apply to a subset of proteins, but not to all. During osmotic oscillations, certain groups of proteins (such as metabolic enzymes) maintained relatively high synthesis rates and hence rose in concentration. By contrast, other proteins – including ribosomal proteins, histones, and cell size regulators – are likely regulated so that their expression scales with growth to maintain their concentrations; the level of accumulation of these proteins during osmotic oscillations would then reflect the robustness of this regulation. Tight control of ribosomal protein concentration is predicted to be another factor to keep the proteome in check [41], preventing accumulation at more rapid rates when expansion is perturbed.

The remarkable cellular phenotype we have presented in which the concentrations of much of the proteome are altered, accompanied by substantial increases in cytoplasmic density that likely involve a sizeable replacement of water within the cytoplasm by protein biomass. Nevertheless, *S. pombe* cells retain viability, grow with normal morphologies, and exhibit normal periods of mitosis and cytokinesis, underscoring the robust control of critical biochemical processes. In particular, this work provides a striking demonstration of how cell size can be maintained even over a 10-fold range of growth rates, a finding inconsistent with models of cell-size control based directly on growth rate [42]. Rather, these results support the existence of cell-size control mechanisms in fission yeast cells that involve direct assessment of cell size through "sizers" [43,44]. In general, our findings indicate that cellular density can be regulated or perturbed in various settings such as stress. Procedures such as osmotic oscillations that increase protein expression per unit volume may have practical applications, for instance in protein production. It will be valuable to explore in future studies the myriad ways in which such global changes in cytoplasmic density affect cellular processes.

410 **METHODS**

411

412 ***Strains and growth conditions***

413 All strains used in this study are listed in Table S1.

414

415 Single colonies were inoculated from plates into liquid rich medium (YE5S, Sunrise Science
416 Products YES-225) overnight with shaking at 30 °C. Once cells reached mid-log phase
417 (OD_{600}~0.5), they were diluted 1:10 directly into ONIX Y04C-02 microfluidic flow cells (EMD
418 Millipore) that had been primed with fresh medium for 15 min. Cells were grown for 15-30 min
419 prior to imaging to allow them to equilibrate to the flow-cell chamber. YE5S was supplemented
420 with D-sorbitol (Sigma) for hypertonic conditions, and fresh medium was introduced into the
421 culture chambers at 5 psi. Control measurements were performed by exchanging YE5S between
422 wells in adjacent culture chambers. By adding a tracer dye (0.5 μg/mL Alexa Fluor 647
423 carboxylic acid; Life Technologies) to the sorbitol-supplemented medium, we determined that
424 media exchange occurred within 10 s (Figure 2A, S3A). Where applicable, drug (cycloheximide
425 or brefeldin A; Sigma) was added to the medium.

426

427 ***Microscopy***

428 Cells were imaged in phase-contrast using a Ti-Eclipse stand (Nikon Instruments) with a 40X
429 (NA: 0.95) or 100X (NA: 1.45) objective, and a Zyla 4.2 sCMOS camera (Andor Technology).
430 Temperature was maintained with a stage-top incubator (OkoLab), which was warmed for at
431 least 1 h prior to imaging. Images were acquired at 1-s or 5-s frame intervals for measuring rapid
432 volume changes during osmotic shocks (Figure S3B), and 1-min or 5-min frame intervals for
433 osmotic shock and growth measurements. For strains expressing fluorescent proteins, cells were
434 imaged in phase-contrast and with laser illumination in spinning-disk confocal mode (Yokogawa
435 CSU-10), and images were acquired with an EM-CCD camera (Hamamatsu) every 10 min at low
436 power to avoid bleaching. The microscope systems were integrated using μManager v. 1.41 [45].

437

438 ***Cell segmentation and size/fluorescence quantification***

439 We first utilized the deep neural network-based machine learning framework *DeepCell* (Van
440 Valen et al., 2017) to segment cells. For each imaging technique (wide-field, confocal) and

441 objective, approximately 200 cells were manually outlined to produce a training dataset. Trained
442 networks were used to generate binary images for feature (extracellular/cell
443 perimeter/cytoplasm) identification. These images were used as the input for gradient
444 segmentation in *Morphometrics* v. 1.1 [46] to define cell contours at sub-pixel resolution.
445
446 The centerline between the two poles was calculated through an iterative method in which
447 symmetric bisections were created starting from the contour's centroid toward the poles. Cell
448 length was defined as the total length of the centerline, and width as the median length of lines
449 running perpendicular to the centerline and stretching between the two sides of the cell. Cell
450 surface area and volume were calculated by integrating disks of revolution at each point on the
451 centerline.
452
453 For fluorescence quantification, the total signal within each cell contour was summed.
454
455 ***Estimation of supergrowth contribution to mCrimson dilution***
456 Estimates for growth-based dilution during supergrowth were calculated using the equation
457
458 $$c_{\text{dilution}}(t) = c_0 + (c_{\max} - c_0)e^{-\int_0^t \frac{1}{V}\frac{dV}{dt}dt},$$
459
460 where the rate of protein production during supergrowth is assumed to follow the growth rate
461 and $\frac{1}{V}\frac{dV}{dt}$ is the population-averaged growth rate. The difference between the actual and
462 estimated concentrations $(c(t) - c_{\text{dilution}}(t))$ was used to estimate the contribution to dilution
463 from growth at >75%.
464
465 ***Bgs4 tip localization and intensity quantification***
466 Cell tips were identified based on peaks in the contour curvature, which is defined at each
467 contour point as the second derivative of the local vector normal. The fluorescence intensity was
468 integrated along a line scan perpendicular to the contour at each contour point whose curvature
469 was greater than 0.12 μm^{-1}, a threshold that was determined visually as an optimal identifier of
470 cell tip regions.

471

472 ***Osmotic oscillations on bulk cultures***

473 Using a tabletop upright glass vacuum filter holder (Fisherbrand) with 0.45-μm HA membrane
474 filters (Millipore, HAWP04700), the medium was rapidly exchanged (<30 s) for cultures of up to
475 200 mL. All media were maintained at 30 °C, and cells were resuspended and shaken at 30 °C
476 during each half-period. One milliliter samples were taken approximately each hour during the
477 experiment and immediately fixed in 70% cold ethanol. Cells from the culture were imaged
478 directly after these oscillations to measure growth rate and mCrimson fluorescence.

479

480 ***Fluorescein isothiocyanate (FITC) and propidium iodide (PI) staining***

481 Staining protocols were adapted from [47]. One-milliliter samples were collected at various time
482 points during the bulk oscillations protocol at $OD_{600} \sim 0.5$, and cells were fixed with 70% cold
483 ethanol for at least 24 h at 4 °C. Approximately 10^6 cells (300 μL) were washed with 50 mM
484 sodium citrate buffer (pH 7.4), and then treated with 0.1 mg/mL RNAse A (ThermoFisher,
485 EN0531) for at least 2 h. For total protein staining, cells were washed and then stained with 5
486 ng/mL FITC (Sigma, F7250) for at least 30 min, then washed three times. To determine total DNA
487 content, cells were stained with PI at 0.1 mg/mL for at least 30 min and then washed.

488

489 To quantify FITC/PI ratios, cells were imaged on 1% agarose + EMM pads (Figure S8). *Z*-stacks
490 were acquired to obtain sum-projections after background subtraction, with cell outlines
491 obtained manually due to the poor phase contrast of fixed cells.

492

493 ***Quantitative Phase Imaging***

494 Images were acquired with a Ti-Eclipse Ti inverted microscope (Nikon) equipped with a 680-nm
495 bandpass filter (D680/30, Chroma Technology) in the illumination path with a 60X (NA: 1.4) DIC
496 oil objective (Nikon). Before imaging, Koehler illumination was configured and the peak
497 illumination intensity with 10-ms exposure time was set to the middle of the dynamic range of
498 the Zyla sCMOS 4.2 camera (Andor). μManager v. 1.41 [45] was used to automate acquisition of
499 brightfield *z*-stacks with a step size of 250 nm from ±3 μm around the focal plane (total of 25
500 imaging planes) at 10-min intervals.

501

502 For analysis, all imaging planes between maximal distances of +1.25 μm and -1.25 μm around the
503 focal plane were selected. Based on these images, the phase information was calculated using a
504 custom Matlab script implementing a previously published algorithm [48]. In brief, this method
505 relates the phase information of the cell to intensity changes along the *z*-direction. Equidistant,
506 out-of-focus images above and below the focal plane are used to estimate intensity changes at
507 various defocus distances. A phase-shift map is reconstructed in a non-linear, iterative fashion to
508 solve the transport-of-intensity equation.
509
510 A Gaussian peak was fitted to the background of each image and then corrected to be at zero
511 phase shift using an image-wide subtraction of the mean of the peak. These corrected images
512 were segmented using *DeepCell* and *Morphometrics* v. 1.1. From the cell outlines, the median
513 intensity of each cell was obtained with ImageJ and used to calculate the cytoplasmic density as
514 follows. The difference of the reconstructed phase map median intensity of cells in YE5S medium
515 compared to cells in YE5S medium supplemented with 100 mg/mL BSA was used to define the
516 phase shift contribution equivalent to 100 mg/mL biomass. The phase shift corresponding to
517 100 mg/mL BSA was then calculated by first averaging the intensity of all cells in YE5S medium
518 at timepoints 10 min before and after BSA addition. Then, the difference relative to the median
519 intensity of all cells during the measurement in YE5S supplemented with 100 mg/mL BSA was
520 defined as the signal contributed by 100 mg/mL biomass.
521
522 Throughout the experiment, multiple measurements in YE5S supplemented with 100 mg/mL
523 BSA were performed and calibration values for each imaging timepoint in between two
524 consecutive measurements in YE5S + BSA were obtained by linear interpolation. These values
525 were then used for quantification of cell density.

AUTHOR CONTRIBUTIONS

B.D.K., K.C.H., and F.C. conceptualized the study. B.D.K., P.O., E.R.R., X.H., K.C.H., and F.C. designed the experiments. B.D.K. and P.O. performed oscillatory osmotic shock experiments. P.O. performed quantitative phase imaging. X.X. and W.C. constructed ribosomal-GFP strains. B.D.K., P.O., E.R.R., K.C.H., and F.C. analyzed data. B.K., K.C.H., and F.C. wrote the manuscript. All authors reviewed the manuscript before submission.

ACKNOWLEDGMENTS

We thank members of the Huang, Chang, J. Skotheim, and S. Dumont labs for helpful discussions. This work was funded by NIH CAREER Award MCB-1149328 (to K.C.H.), the Allen Discovery Center at Stanford University on Systems Modeling of Infection (to K.C.H.), the National Natural Science Foundation of China (NSFC; 3167080548) (to X.H.), and NIH R01-GM56836 and Bilateral BBSRC-NSF/BIO Award 1638195 (to F.C.). K.C.H. is a Chan Zuckerberg Biohub Investigator.

FIGURE LEGENDS

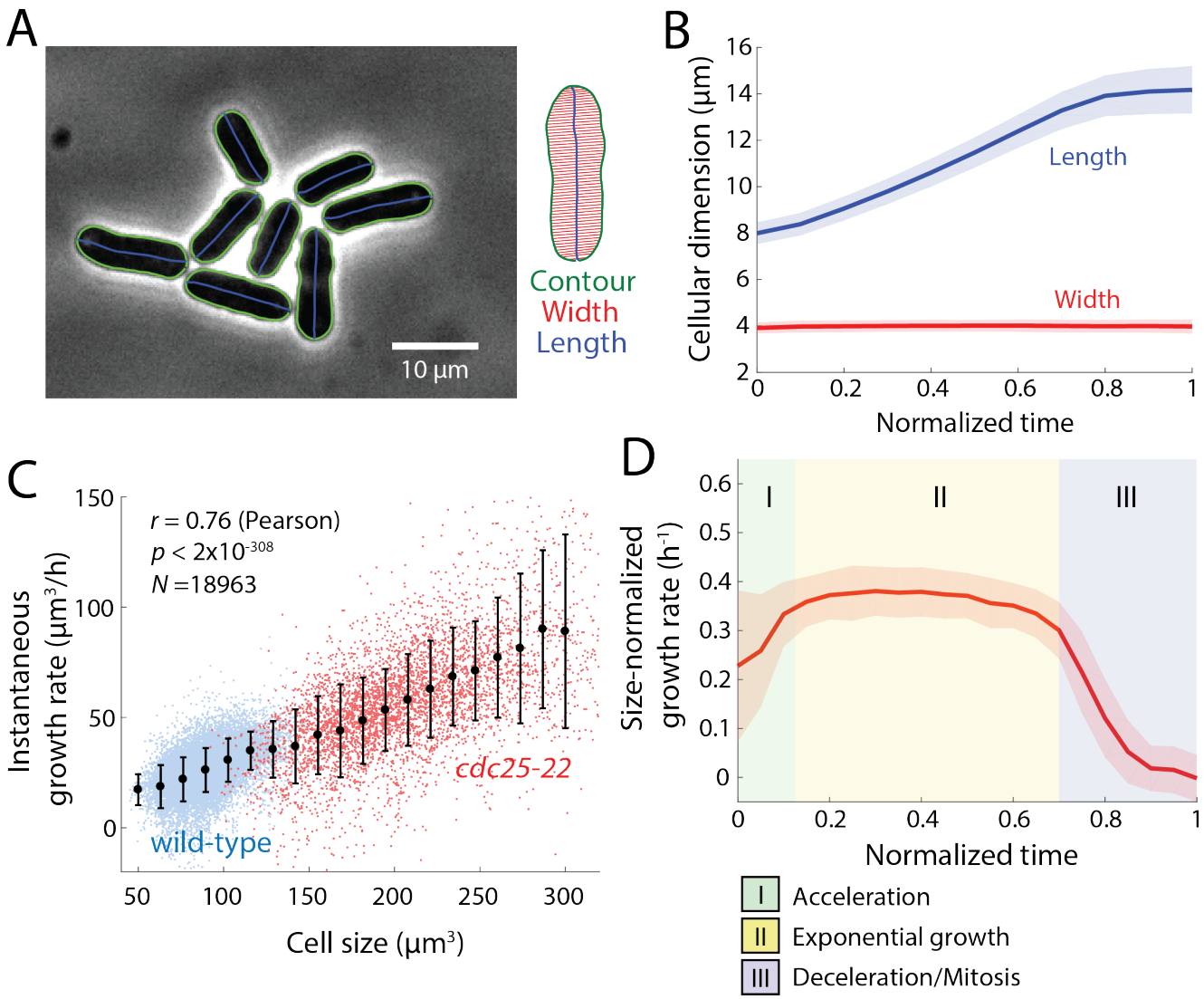

Figure 1: *S. pombe* cells grow exponentially.

A) Wild-type (WT) fission yeast cells imaged in phase contrast. Green outlines were obtained via automated segmentation (Methods). Manual inspection revealed that segmentation was accurate for virtually all cells, regardless of cell crowding.

B) Population-averaged length and width of growing fission yeast cells, measured as a function of time after the mechanical separation of daughter cells after septation normalized by cell-cycle time (n = 1129 cells). Solid lines and shaded areas represent the mean ± 1 standard deviation (S.D.). Cell width was essentially invariant, while

length increased over the cell cycle until the cell reaches the division length of ~14 μm.

C) Instantaneous growth rate dL/dt increased with cell length. The trend for wild-type (WT) cells (blue) continued for *cdc25-22* cells (red), which are substantially longer. Black lines represent best linear fits for each strain (wildtype, *n*=1129 cells; *cdc25-22*, *n*=246 cells).

D) Instantaneous size-normalized growth rate $\left(\frac{1}{L}dL/dT\right)$ of wild-type cells, as a function of normalized cell-cycle time as in (B). The size-normalized growth rate was constant for a large fraction of the cell cycle, signifying growth proportional to size (exponential growth). Cells had three phases of growth: (I) super-exponential acceleration, (II) steady-state exponential growth, and (III) deceleration as cells approach mitosis.

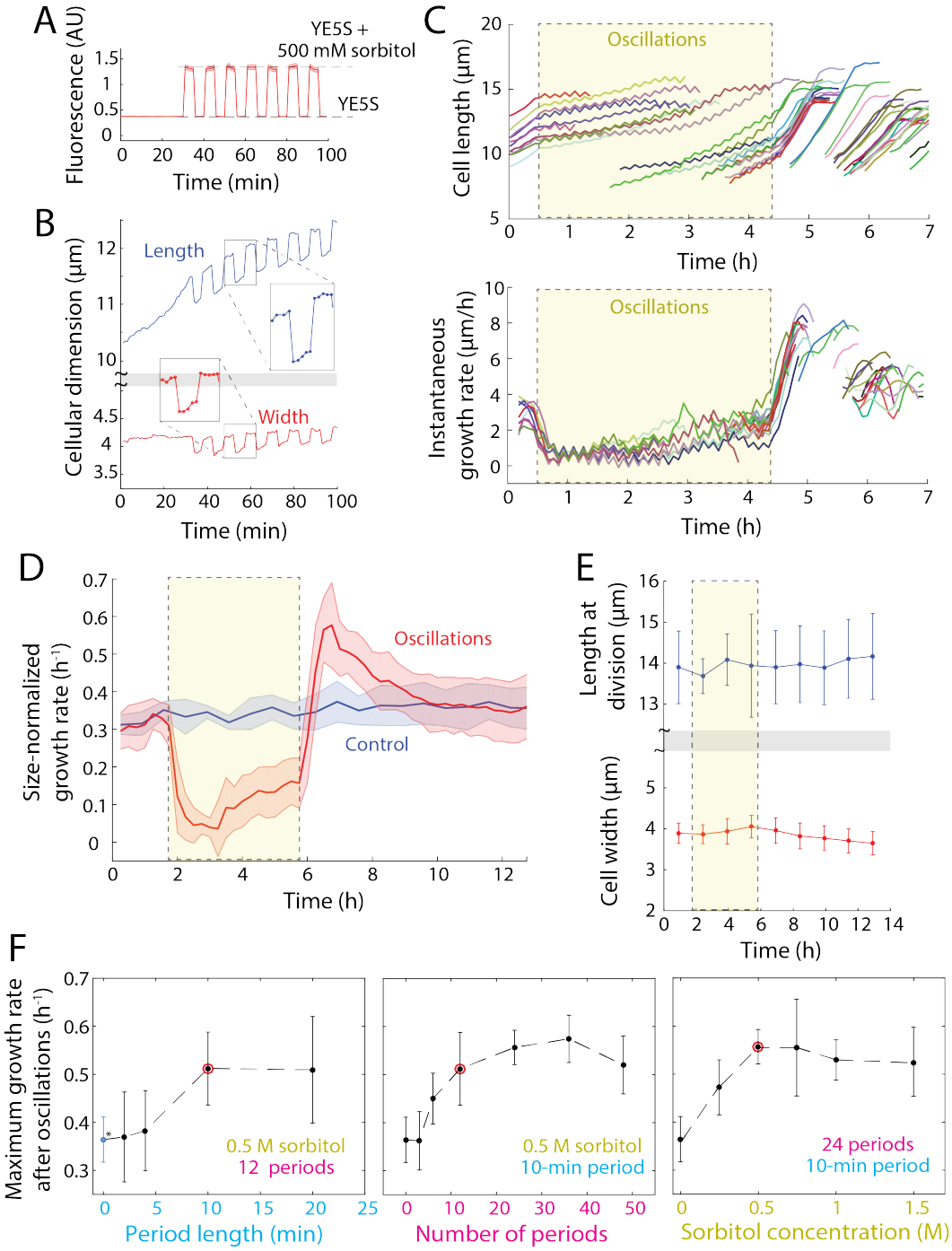

Figure 2: Exit from osmotic shock oscillations induces robust supergrowth.

A) Cells were equilibrated to achieve steady-state growth in YE5S, and then exposed to cycles of hyperosmotic and hypoosmotic shocks with 500 mM sorbitol, with 5 min between shocks.

B) Length of a representative wild-type (WT) cell increased more rapidly during periods in YE5S+500 mM sorbitol, but returned to the value expected of growth in YE5S after

570 hypoosmotic shocks. Width increased in YE5S+500 mM sorbitol, and was maintained at
571 an approximately constant level in YE5S.
572 C) Length (top) and instantaneous growth rates (bottom) of wild-type cells (n = 45) before,
573 during (yellow shading), and after 24 cycles of 0.5-M sorbitol osmotic shock oscillations
574 with 10-min period. Cells are the same color in both plots. Cells were imaged every 5 min.
575 After the oscillations, cells exhibited faster growth (supergrowth) for multiple
576 generations. Traces that begin at later times points are newly formed daughter cells.
577 D) Size growth rates of wild-type cells throughout an oscillatory osmotic shock experiment
578 (red, n = 973 cells). Growth rate during oscillations (yellow, dashed box) was lower than
579 the control that was kept in YE5S throughout (blue, n = 1242). Growth rate increased
580 after cells exited the oscillations, decreasing back to the control growth rate with a time
581 constant of 1.3 h.
582 E) Cell-size control was unaffected by oscillations or supergrowth, with constant length (top)
583 and width (bottom) at the time of division throughout the experiment in (C).
584 F) Maximal size-normalized growth rates during supergrowth as a function of (i) oscillatory
585 shock period length, (ii) number of periods, and (iii) sorbitol concentration (n = 46-536
586 cells per data point). Each parameter was varied while the other two parameters were
587 held fixed. Red circles represent our standard conditions of 24 cycles of 500-mM shocks
588 with 10-min period. Error bars represent one standard deviation.
589

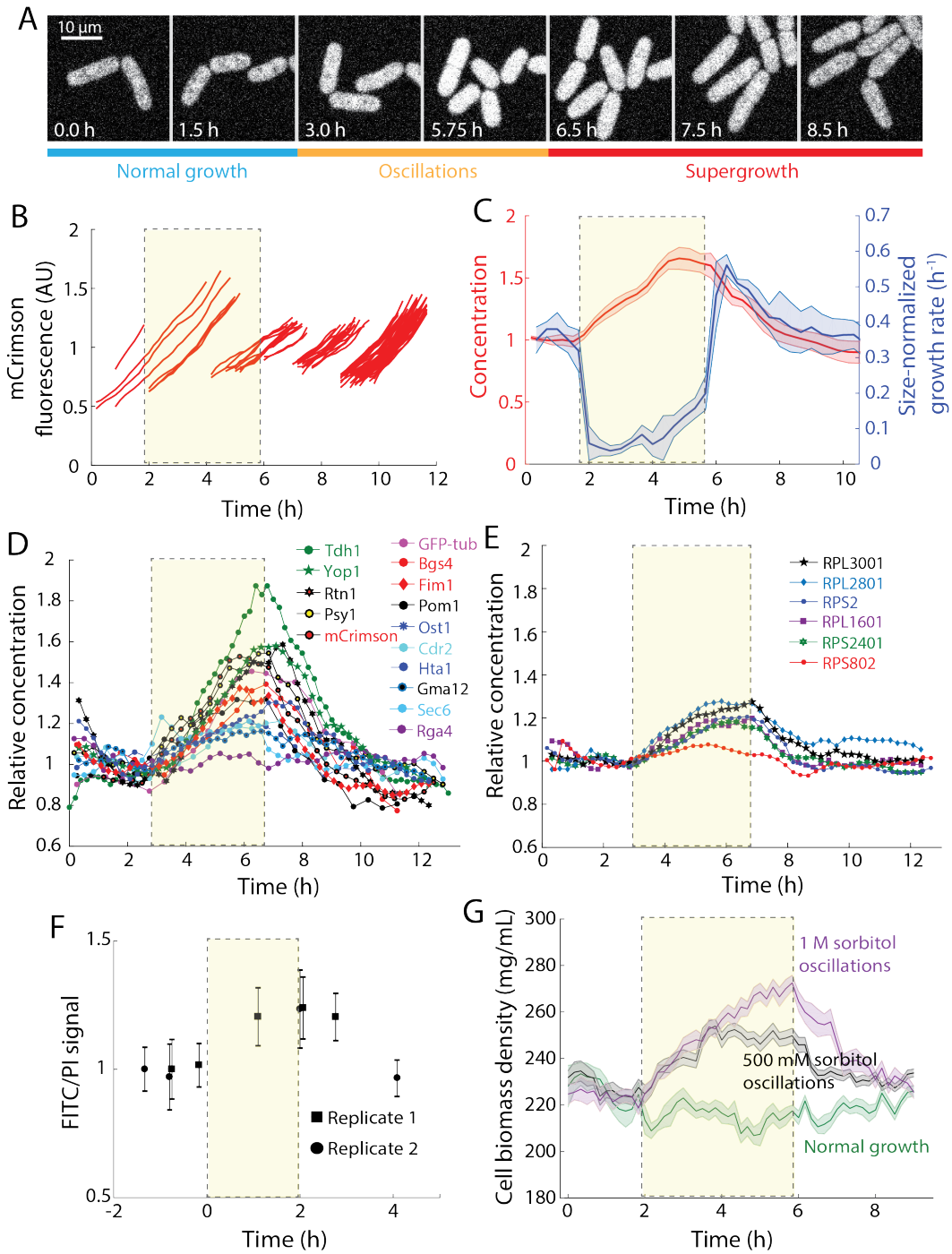

Figure 3: Osmotic-shock oscillations disrupt coupling between protein synthesis and cell size.

A) Representative time-lapse images of mCrimson-expressing cells before, during, and after 24 10-min periods of 0.5-M sorbitol osmotic shocks. Fluorescence intensity

increased during oscillations, and then gradually reverted to pre-shock levels during supergrowth.

B) Representative trajectories of integrated cellular fluorescence before, during, and after oscillations (*n* =54 cells). Synthesis of mCrimson continued relatively unabated during oscillations. The yellow box in this and subsequent panels denotes the 24 10-min periods of 0.5-M sorbitol osmotic shocks. (n = 54 cells)

C) mCrimson concentration increases by ~60% during oscillations (red), despite large decreases in volume growth rate (blue) (*n* = 843 cells). During supergrowth, the increased growth rate led to dilution of the mCrimson concentration. Dark centerline is the population-averaged mean, and the shading represents one standard deviation.

D) Concentrations of various proteins labeled with fluorescent proteins before, during, and after oscillations. All protein concentrations increased during oscillations, but to varying degrees.

E) Ribosomal proteins also increased during oscillations, but to a lesser degree; RPS802 concentration remained approximately constant throughout the experiment.

F) The ratio of FITC (proteins) to PI (DNA) fluorescence, a proxy for global protein density, increased during oscillations and then decreased back to steady-state levels during supergrowth. Cells were subjected to 12 cycles of 500-mM sorbitol shocks with 10-min period (Methods). Error bars are one standard deviation (*n* = 200 cells each datapoint).

G) Cytoplasmic density, as measured by quantitative phase imaging (Methods), increased during osmotic shocks and decreased during supergrowth. Dark centerline is the population-averaged mean cell density, and the shading represents one standard deviation. Green: normal growth (*n* = 88 cells); black, 500-mM oscillations (*n* = 187 cells); purple, 1-M oscillations (*n* = 106 cells).

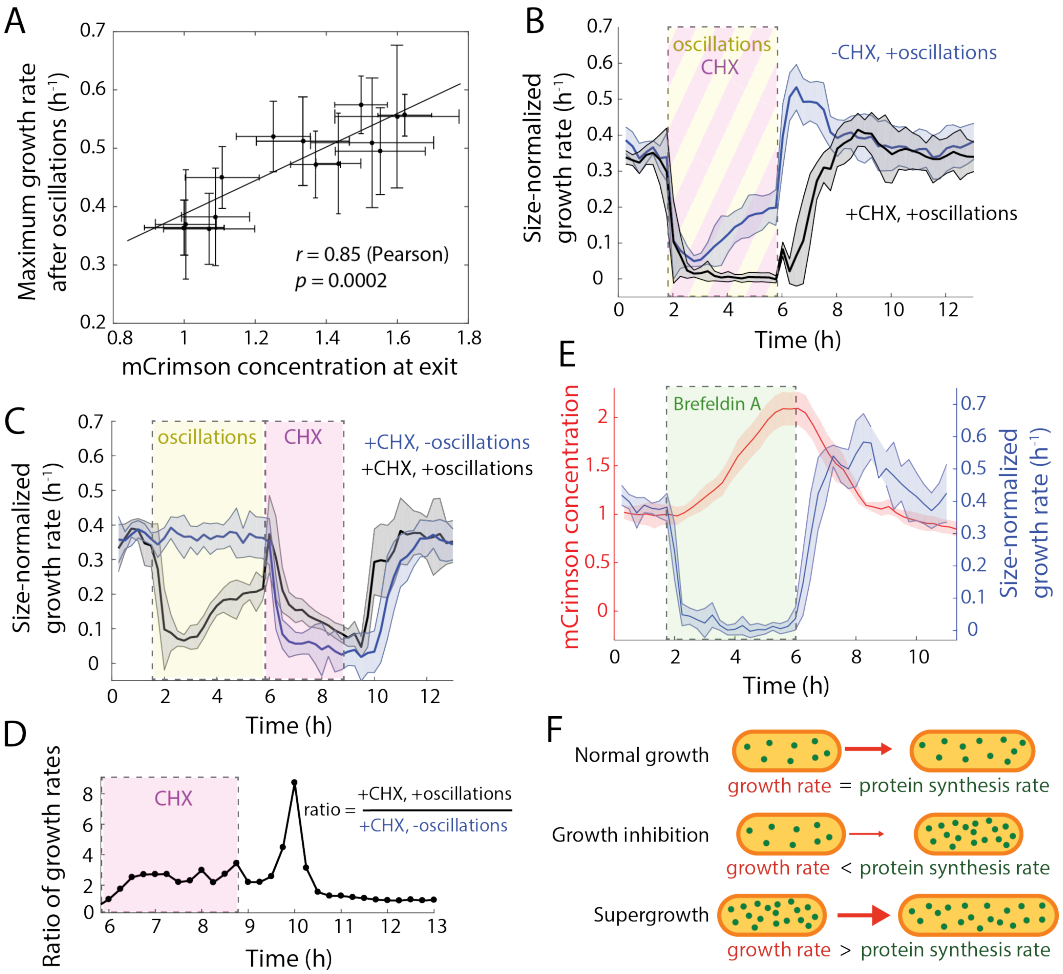

Figure 4: Excess protein concentration is necessary for supergrowth.

A) Maximum size-normalized growth rates were highly correlated with the mean mCrimson concentration at exit from oscillations, across all shock magnitudes, periods, and number of shock cycles in Figure 2F. Error bars represent one standard deviation.

B) Cells treated with 100 μg/mL of the translation inhibitor cycloheximide (CHX; black shading, n = 228 cells) during oscillations (24 10-min periods, 0.5-M sorbitol shocks; yellow shading) rapidly halted growth during oscillations and exhibited no supergrowth afterward, unlike untreated cells (blue, n = 545 cells). Shading represents one standard deviation.

C) Cells exposed to osmotic-shock oscillations as in (B) (black, n = 175 cells) or maintained in constant YE5S growth conditions (blue, n = 260 cells) were treated (directly after the exit from oscillations) for 3 h with 100 μg/mL cycloheximide. Cells

635 that underwent oscillations grew more during CHX treatment and resumed normal
636 growth more quickly after CHX washout. Shading represents one standard deviation.
637 D) During cycloheximide treatment, the ratio of growth rates of cells that did and did not
638 undergo oscillations was always ≥1 and reached a plateau within 30 min. At the
639 plateau, cells that underwent oscillations grew approximately three-fold faster than
640 control cells. The growth-rate ratio remained >1 for 2-3 h after cycloheximide
641 treatment.
642 E) Brefeldin A (green shading) treatment completely inhibited growth, while mCrimson
643 continued to accumulate throughout treatment. After the drug was washed out, cells
644 initiated supergrowth with dynamics similar to those achieved after osmotic shocks.

645 **REFERENCES**

646

647 1 Newman, J. R. *et al.* Single-cell proteomic analysis of S. cerevisiae reveals the architecture
648 of biological noise. *Nature* **441**, 840-846, doi:10.1038/nature04785 (2006).
649 2 Schmoller, K. M., Turner, J. J., Koivomagi, M. & Skotheim, J. M. Dilution of the cell cycle
650 inhibitor Whi5 controls budding-yeast cell size. *Nature* **526**, 268-272,
651 doi:10.1038/nature14908 (2015).
652 3 Zhou, X. *et al.* Bacterial division. Mechanical crack propagation drives millisecond
653 daughter cell separation in Staphylococcus aureus. *Science* **348**, 574-578,
654 doi:10.1126/science.aaa1511 (2015).
655 4 You, C. *et al.* Coordination of bacterial proteome with metabolism by cyclic AMP
656 signalling. *Nature* **500**, 301-306, doi:10.1038/nature12446 (2013).
657 5 Padovan-Merhar, O. *et al.* Single mammalian cells compensate for differences in cellular
658 volume and DNA copy number through independent global transcriptional mechanisms.
659 *Mol Cell* **58**, 339-352, doi:10.1016/j.molcel.2015.03.005 (2015).
660 6 Willis, L. & Huang, K. C. Sizing up the bacterial cell cycle. *Nat Rev Microbiol* **15**, 606-620,
661 doi:10.1038/nrmicro.2017.79 (2017).
662 7 Tzur, A., Kafri, R., LeBleu, V. S., Lahav, G. & Kirschner, M. W. Cell growth and size
663 homeostasis in proliferating animal cells. *Science* **325**, 167-171,
664 doi:10.1126/science.1174294 (2009).
665 8 Abenza, J. F. *et al.* Wall mechanics and exocytosis define the shape of growth domains in
666 fission yeast. *Nat Commun* **6**, 8400, doi:10.1038/ncomms9400 (2015).
667 9 Chang, F. & Martin, S. G. Shaping fission yeast with microtubules. *Cold Spring Harb*
668 *Perspect Biol* **1**, a001347, doi:10.1101/cshperspect.a001347 (2009).
669 10 Atilgan, E., Magidson, V., Khodjakov, A. & Chang, F. Morphogenesis of the Fission Yeast Cell
670 through Cell Wall Expansion. *Curr Biol* **25**, 2150-2157, doi:10.1016/j.cub.2015.06.059
671 (2015).
672 11 Mitchison, J. M. & Nurse, P. Growth in cell length in the fission yeast Schizosaccharomyces
673 pombe. *J Cell Sci* **75**, 357-376 (1985).

674 12 Baumgartner, S. & Tolic-Norrelykke, I. M. Growth pattern of single fission yeast cells is
675 bilinear and depends on temperature and DNA synthesis. *Biophys J* **96**, 4336-4347,
676 doi:10.1016/j.bpj.2009.02.051 (2009).
677 13 Sveiczer, A., Novak, B. & Mitchison, J. M. The size control of fission yeast revisited. *J Cell Sci*
678 **109 (Pt 12)**, 2947-2957 (1996).
679 14 Cooper, S. Distinguishing between linear and exponential cell growth during the division
680 cycle: single-cell studies, cell-culture studies, and the object of cell-cycle research. *Theor*
681 *Biol Med Model* **3**, 10, doi:10.1186/1742-4682-3-10 (2006).
682 15 Horvath, A., Racz-Monus, A., Buchwald, P. & Sveiczer, A. Cell length growth patterns in
683 fission yeast reveal a novel size control mechanism operating in late G2 phase. *Biol Cell*
684 **108**, 259-277, doi:10.1111/boc.201500066 (2016).
685 16 Horvath, A., Racz-Monus, A., Buchwald, P. & Sveiczer, A. Cell length growth in fission yeast:
686 an analysis of its bilinear character and the nature of its rate change transition. *FEMS*
687 *Yeast Res* **13**, 635-649, doi:10.1111/1567-1364.12064 (2013).
688 17 Chang, F., Atilgan, E., Burgess, D. & Minc, N. Manipulating cell shape by placing cells into
689 micro-fabricated chambers. *Methods Mol Biol* **1136**, 281-290, doi:10.1007/978-1-4939-
690 0329-0_13 (2014).
691 18 Basu, R., Munteanu, E. L. & Chang, F. Role of turgor pressure in endocytosis in fission
692 yeast. *Mol Biol Cell* **25**, 679-687, doi:10.1091/mbc.E13-10-0618 (2014).
693 19 Minc, N., Boudaoud, A. & Chang, F. Mechanical forces of fission yeast growth. *Curr Biol* **19**,
694 1096-1101, doi:10.1016/j.cub.2009.05.031 (2009).
695 20 Proctor, S. A., Minc, N., Boudaoud, A. & Chang, F. Contributions of turgor pressure, the
696 contractile ring, and septum assembly to forces in cytokinesis in fission yeast. *Curr Biol*
697 **22**, 1601-1608, doi:10.1016/j.cub.2012.06.042 (2012).
698 21 Rojas, E., Theriot, J. A. & Huang, K. C. Response of Escherichia coli growth rate to osmotic
699 shock. *Proc Natl Acad Sci U S A* **111**, 7807-7812, doi:10.1073/pnas.1402591111 (2014).
700 22 Chen, D. *et al.* Global transcriptional responses of fission yeast to environmental stress.
701 *Mol Biol Cell* **14**, 214-229, doi:10.1091/mbc.E02-08-0499 (2003).
702 23 Sanchez-Mir, L. *et al.* Rho1 GTPase and PKC Ortholog Pck1 Are Upstream Activators of the
703 Cell Integrity MAPK Pathway in Fission Yeast. *Plos One* **9**, doi:ARTN e88020
704 10.1371/journal.pone.0088020 (2014).

705 24 Ma, Y. *et al.* Transient receptor potential (TRP) and Cch1-Yam8 channels play key roles in
706 the regulation of cytoplasmic Ca2+ in fission yeast. *PLoS One* **6**, e22421,
707 doi:10.1371/journal.pone.0022421 (2011).
708 25 Davie, E., Forte, G. M. & Petersen, J. Nitrogen regulates AMPK to control TORC1 signaling.
709 *Curr Biol* **25**, 445-454, doi:10.1016/j.cub.2014.12.034 (2015).
710 26 Schutt, K. L. & Moseley, J. B. Transient activation of fission yeast AMPK is required for cell
711 proliferation during osmotic stress. *Molecular Biology of the Cell* **28**, 1804-1814,
712 doi:10.1091/mbc.E17-04-0235 (2017).
713 27 Ikeda, K., Morigasaki, S., Tatebe, H., Tamanoi, F. & Shiozaki, K. Fission yeast TOR complex 2
714 activates the AGC-family Gad8 kinase essential for stress resistance and cell cycle control.
715 *Cell Cycle* **7**, 358-364, doi:10.4161/cc.7.3.5245 (2008).
716 28 Al-Sady, B., Greenstein, R. A., El-Samad, H. J., Braun, S. & Madhani, H. D. Sensitive and
717 Quantitative Three-Color Protein Imaging in Fission Yeast Using Spectrally Diverse,
718 Recoded Fluorescent Proteins with Experimentally-Characterized In Vivo Maturation
719 Kinetics. *Plos One* **11**, doi:ARTN e0159292
720 10.1371/journal.pone.0159292 (2016).
721 29 Waldron, C. & Lacroute, F. Effect of Growth-Rate on Amounts of Ribosomal and Transfer
722 Ribonucleic-Acids in Yeast. *J Bacteriol* **122**, 855-865 (1975).
723 30 Polanshek, M. M. Effects of heat shock and cycloheximide on growth and division of the
724 fission yeast, Schizosaccharomyces pombe. With an Appendix. Estimation of division
725 delay for S. pombe from cell plate index curves. *J Cell Sci* **23**, 1-23 (1977).
726 31 Cortes, J. C. *et al.* The novel fission yeast (1,3)beta-D-glucan synthase catalytic subunit
727 Bgs4p is essential during both cytokinesis and polarized growth. *J Cell Sci* **118**, 157-174,
728 doi:10.1242/jcs.01585 (2005).
729 32 Mutavchiev, D. R., Leda, M. & Sawin, K. E. Remodeling of the Fission Yeast Cdc42 Cell-
730 Polarity Module via the Sty1 p38 Stress-Activated Protein Kinase Pathway. *Curr Biol* **26**,
731 2921-2928, doi:10.1016/j.cub.2016.08.048 (2016).
732 33 Haupt, A., Ershov, D. & Minc, N. A Positive Feedback between Growth and Polarity
733 Provides Directional Persistency and Flexibility to the Process of Tip Growth. *Current*
734 *Biology* **28**, 3342-+, doi:10.1016/j.cub.2018.09.022 (2018).

735 34 Novick, P., Field, C. & Schekman, R. Identification of 23 complementation groups required
736 for post-translational events in the yeast secretory pathway. *Cell* **21**, 205-215 (1980).
737 35 Brazer, S. C., Williams, H. P., Chappell, T. G. & Cande, W. Z. A fission yeast kinesin affects
738 Golgi membrane recycling. *Yeast* **16**, 149-166, doi:10.1002/(SICI)1097-
739 0061(20000130)16:2<149::AID-YEA514>3.0.CO;2-C (2000).
740 36 Lippincottschwartz, J., Yuan, L. C., Bonifacino, J. S. & Klausner, R. D. Rapid Redistribution of
741 Golgi Proteins into the Er in Cells Treated with Brefeldin-a - Evidence for Membrane
742 Cycling from Golgi to Er. *Cell* **56**, 801-813, doi:Doi 10.1016/0092-8674(89)90685-5
743 (1989).
744 37 Cleveland, D. & Kirschner, M. Autoregulatory control of the expression of alpha- and beta-
745 tubulins: implications for microtubule assembly. *Cold Spring Harb Symp Quant Biol* **46 Pt**
746 **1**, 171-183 (1982).
747 38 Springer, M., Weissman, J. S. & Kirschner, M. W. A general lack of compensation for gene
748 dosage in yeast. *Mol Syst Biol* **6**, 368, doi:10.1038/msb.2010.19 (2010).
749 39 Torres, E. M., Springer, M. & Amon, A. No current evidence for widespread dosage
750 compensation in S. cerevisiae. *Elife* **5**, e10996, doi:10.7554/eLife.10996 (2016).
751 40 Torres, E. M. *et al.* Effects of aneuploidy on cellular physiology and cell division in haploid
752 yeast. *Science* **317**, 916-924, doi:10.1126/science.1142210 (2007).
753 41 Zhao, Y., Sohn, J. H. & Warner, J. R. Autoregulation in the biosynthesis of ribosomes. *Mol*
754 *Cell Biol* **23**, 699-707 (2003).
755 42 Lucena, R. *et al.* Cell Size and Growth Rate Are Modulated by TORC2-Dependent Signals.
756 *Curr Biol* **28**, 196-210 e194, doi:10.1016/j.cub.2017.11.069 (2018).
757 43 Pan, K. Z., Saunders, T. E., Flor-Parra, I., Howard, M. & Chang, F. Cortical regulation of cell
758 size by a sizer cdr2p. *Elife* **3**, e02040, doi:10.7554/eLife.02040 (2014).
759 44 Facchetti, G., Chang, F. & Howard, M. Controlling cell size through sizer mechanisms.
760 *Current Opinion in Systems Biology* **5**, 86-92,
761 doi:https://doi.org/10.1016/j.coisb.2017.08.010 (2017).
762 45 Edelstein, A. D. *et al.* Advanced methods of microscope control using μManager software.
763 *Journal of biological methods* **1**, e10 (2014).

764 46 Ursell, T. *et al.* Rapid, precise quantification of bacterial cellular dimensions across a
765 genomic-scale knockout library. *BMC Biol* **15**, 17, doi:10.1186/s12915-017-0348-8
766 (2017).
767 47 Porro, D., Brambilla, L. & Alberghina, L. Glucose metabolism and cell size in continuous
768 cultures of Saccharomyces cerevisiae. *FEMS Microbiol Lett* **229**, 165-171 (2003).
769 48 Bostan, E., Froustey, E., Nilchian, M., Sage, D. & Unser, M. Variational Phase Imaging Using
770 the Transport-of-Intensity Equation. *IEEE Trans Image Process* **25**, 807-817,
771 doi:10.1109/TIP.2015.2509249 (2016).
772